Predominant cellular mitochondrial dysfunction in the *TOP3A* gene caused Bloom syndrome-like disorder

Wenjun JIANG
Shanghai Jiaotong University School of Medicine Xinhua Hospital
Nan JIA
Guangzhou Medical College First Affiliated Hospital
Chaowan GUO
Nagoya University: Nagoya Daigaku
Juan WEN
Central South University
Lingqian WU
Central South University
Tomoo OGI
Nagoya University: Nagoya Daigaku
Huiwen Zhang (zhanghuiwen@xinhuamed.com.cn)
Shanghai Jiao Tong University School of Medicine Affiliated Xin Hua Hospital https://orcid.org/0000-0002-8241-325X

Research

Keywords: TOP3A, Bloom-like syndrome, Genome instability, Mitochondria dysfunction

Posted Date: September 3rd, 2020

DOI: https://doi.org/10.21203/rs.3.rs-67767/v1

Version of Record: A version of this preprint was published at Biochimica et Biophysica Acta (BBA) - Molecular Basis of Disease on June 1st, 2021. See the published version at https://doi.org/10.1016/j.bbadis.2021.166106.

Abstract

Background

TOP3A is a subunit of the BLM-TOP3A-RMI1/2 complex, which promotes processing of double Holliday junction dissolution and also plays an important role in decatenation and segregation of human mtDNA. Recently, *TOP3A* mutations have been reported to cause Bloom syndrome-like disorder. However, whether the two function play equal roles in the disease pathogenesis is unclear.

Results

Beside the common clinical manifestations in the reported TOP3A-deficiency, our patients also exhibited liver lipid storage with hepatomegaly and elevated liver enzyme. In cellular and molecular biological studies, *TOP3A* deficiency decreased the cellular protein level of RMI1 and RMI2, and moderately increased sister chromatid exchanges and decreased cell proliferation compared with BLM or RMI2 deficiency. These changes were rescued by ectopic expression of either of the wildtype TOP3A or TOP3A-D479G. In contrast, reduced mitochondrial ATP generation and oxygen consumption rates observed in *TOP3A* defective cells were rescued by over-expression of the wildtype TOP3A, but not TOP3A-D479G.

Conclusions

Considering the severe disease course and the impact of the TOP3A-D479G mutation on the genome stability and mitochondrial metabolism, we propose that the impaired mitochondrial metabolism plays an important role in the pathogenesis of TOP3A-deficient Bloom-like disease.

1. Background

Bloom syndrome, first described in 1966[1, 2], is characterized by proportionate pre- and postnatal growth retardation, sun-sensitive skin, and predisposition to malignancy, which are due to mutations in the *BLM* gene. The *BLM* gene encodes for the DNA repair enzyme, RecQL3 helicase, which is critical for chromosomal stability. Typical Bloom syndrome cases are usually easily recognized clinically. However, it could be a challenging diagnosis when photosensitive skin lesions had not been fully developed or even absent[3, 4]. Despite predisposition to malignancy, patients with Bloom syndrome could give birth to healthy children under surveillance[5].

The BLM helicase, along with RecQ-mediated genome instability proteins (RMI1/2) and topoisomerase III alpha (TOP3A), forms a protein complex (BTR complex) that promotes the dissolution of double Holliday junctions (dHJs) throughout the cell cycle and is crucial for genome stability[6–12]. Defects in BTR complex generate more crossover products that can be visualized as increased sister chromatid exchanges (SCEs). Cells derived from *BLM*-deficient individuals show more SCEs and genome instability[13, 14]. Recently, individuals with balletic mutations in *RMI1*, *RMI2*, or *TOP3A*, had been described as Bloom syndrome-like disorder[15, 16]. In total, 11 individuals with *TOP3A* deficiency-induced Bloom syndrome-like disorder caused by 8 different *TOP3A* mutations had been reported. Most *TOP3A* affected individuals, as well as two *RMI2* deficient patients, are reported with increased SCEs. Independent from its nuclear role, TOP3A exists in its mitochondrial form and play important role in mitochondrial DNA (mtDNA) replication, decatenation, and segregation machinery[17, 18]. Several patients with *TOP3A* deficiency also presented clinical features of mitochondrial dysfunction, such as chronic progressive external ophthalmoplegia. The pathological mechanism and the treatment options of *TOP3A* deficiency need to be further elucidated[17, 19].

Here we report *TOP3A* deficiency in two siblings with pre- and postnatal growth retardation, microcephaly, decreased subcutaneous fat, dilated cardiomyopathy, as well as with new clinical features, including hepatomegaly with liver lipid storage and elevated liver enzyme. We also demonstrate that the impact of the missense mutation, TOP3A-D479G, on mitochondrial energy metabolism is more evident than on the genome stability in HCT116 cells.

2. Results

2.1. Bloom-like syndrome patients have a compound heterozygous mutation in TOP3A

A non-consanguineous couple with above average height (father 175 cm, mother 165 cm) gave birth to two children with similar clinical features (Fig. 1a). The older brother presented severe pre- and postnatal growth retardation. Routine prenatal checkups by ultrasound revealed a restricted fetal growth, which persisted to the birth, while the amniotic fluid volume, umbilical cord, and the morphology of uterus were unremarkable. At about month 7 of pregnancy, the boy was born by a spontaneous vaginal delivery with birth weight of 1.5 kg. Afterward, the boy had poor appetite and slow growth.

At 2-years-old, his height was 74.9 cm, weight was 6.1 kg, and occipitofrontal head circumference was 43 cm. At this age, he was also observed to have triangular face, thin subcutaneous fat, and straight nose bridge. Despite the growth retardation, the boy had near normal motor and language developments. He began to walk independently after 1 year. At 2 years, he could run and hop. The endoscopy of stomach and echocardiography were undergone for poor appetite and turned to be unremarkable. All blood biochemical tests including liver function, glucose, blood lipids, and lactate, as well as the karyotype were normal. A negative result with SALSA MLPA ME030 BWS/RSS probemix (ME030, MRC-Holland) excluded likelihood of Silver-Russell Syndrome.

At 2 years 2 months, the boy started growth hormone treatment. His height increased to 89 cm, and weight increased to 11 kg at 3 years 5 months. The treatment was stopped immediately when increased ALT (159 IU/L) and AST (75 IU/L) levels were found. After that, multiple tests revealed mildly elevated liver enzyme with mildly elevated AFP (17.9 IU/L), and hepatomegaly was observed with fine echo pattern, which prompted a liver biopsy with fatty liver revealed. In the following months, acanthosis nigricans was observed in the skin of neck, armpits, and groin area. However, an oral glucose tolerance test revealed normal insulin secretion and blood lipid kept normal. Ursodeoxycholic acid and polyenephosphatidyl choline had been tried sequentially to protect hepatocytes, but failed to do so.

At 6 years 2 months, echocardiography revealed enlargement of left atrial and ventricular and heart failure when the patients had recurrent cough, shortness of breath and fatigue. He died 6 months later for heart failure (6 years and 8 months old). His growth parameters are shown in **Supplemental Fig. 4a-c.**

The sister was found to be small at month 5 of pregnancy **(**Fig. 1b**)**. She was born full term by a spontaneous vaginal delivery with birth weight of 1.5 kg. The known growth parameters are shown in **Supplemental Fig. 4d-f.** Most of the time, she had very poor appetite and grew very slowly while maintaining a roughly normal intelligence. She was treated with growth hormones for three months, which was discontinued after finding mildly increased AFP (15.4 IU/L), although normal ALT (34 IU/L) and AST (42 IU/L) levels and an unpalpable liver at right costal margin at 3 years 4 months. Six months later, her liver was observed with fine echo pattern and no abnormality was found by echocardiography. Another one and half years later, when she was 5 years and 4 months old, she also found to have enlargement of left atrial and ventricular and heart failure. Without heart-protection drugs, her situation deteriorated rapidly and she died in two weeks (5 years and 6 months old).

Whole exome sequencing was carried out on the brother and the sister and three potentially pathogenic candidate genes were identified, *TOP3A, GOLGA6L1*, and *GOLGA6L22*. *TOP3A* was the most likely to be linked to the above pathologic findings. One mutation (c.2362C > T, p.Q788*) derived from the father introduced a premature stop codon and located in the non-function region of *TOP3A*; the second mutation (c.1436A > G, p.D479G) was a missense mutation and was located at a highly conserved residue in eukaryotes within the TOPA domain (Fig. 1c, d), and would, therefore, be expected to be crucial for the enzymatic activity of the TOP3A protein.

To test the expression of mutated *TOP3A* gene products, an allele-specific quantitative RT-PCR was carried out, which revealed relatively low expression of the p.Q778* allele and the allele encompassing p.D479G missense mutation (designated as TOP3A-D479G hereafter) (Fig. 1e). Cell lines deviated from the patient peripheral blood were unavailable. We could not examine the exact expression level of the mutated TOP3A proteins. Given the above results and that *TOP3A* gene is essential for the early stage of development in mice[21], we expected that two identified mutations result in low cellular TOP3A protein level and marked decrease of function of TOP3A in patients cells.

3.2 TOP3A loss moderately affects sister chromatid exchange and cell proliferation but not UV sensitivity

Cells derived from *TOP3A* deficiency individuals were reported with elevated sister chromatid exchanges (SCEs), which is a typical characteristic of Bloom-like syndrome[15]. To investigate whether the affected patients in this study carry the similar cytological phenotype, fresh blood samples collected from the sister and an age-matched control were assayed microscopically for SCE events. Fifteen cells from each individual were examined. As shown in Fig. 2a and 2b, a marked increase of SCEs (~ 4.0-fold) was observed in patient cells, with a mean of 19.8 SCEs/cell in patient cells compared with a mean of 5 SCEs/cells in control cells, indicating defective BTR complex function in the sister.

Cytological analysis with fibroblast cell lines was also performed with generated isogenic *TOP3A* gene knockout cell lines in HCT116 using the CRISPR/cas9 gene editing technique. Gene targeting guide RNAs designed on exon regions of the *TOP3A*, as well as *BLM*, or *RMI2* genes were used to generate knockout cell lines. For each gene of interest, two knockout cell lines were isolated and used in the subsequent functional studies; the detail information of guide RNA and the mutations in each gene were shown in **Supplemental Fig. 2a-c**. Gene knockout effects of generated cell lines were confirmed by immunoblotting. Knockout of the *TOP3A* gene largely reduced the cellular protein level of RMI1 and RMI2 but did not significantly affect BLM (Fig. 2c, **left**). However, knockout of *RMI2* significantly decrease TOP3A and RMI1 levels (Fig. 2c, **right**). On the other hand, knockout of the *BLM* gene did not significantly change RMI1, RMI2, or TOP3A protein levels. Consistent with the former report, these results indicate strong association among TOP3A, RMI1, and RMI2, regardless of the presence or absence of BLM[6].

BTR complex defects in mitotic cells impact homologous recombination (HR), which subsequently affects cell viability and proliferation. To confirm whether loss of *TOP3A* affected the cell proliferation, we tested the growth curve with each knock out cell line, which were seeded in dishes and grown for 5 days before harvest and counting. As shown in Fig. 3a, the $BLM^{-/-}$ cells displayed a significant slowing down in cell proliferation, as indicated in Groden's work[22]. Compared to the wildtype HCT116 cells, a detectable decrease in cell growth rate was shown in $TOP3A^{-/-}$ cells, as well as in $RMI2^{-/-}$ cells, which is consistent with a previous report[16].

The frequency of SCEs was detected with the HCT116 knockout cell lines (Fig. 3b and 3c). The HCT116 $TOP3A^{-/-}$ cells showed an approximate 3.2-fold increase compared to wild type HCT116 cells ($p < 0.0001$), with an average of 19.8 and 6.2 SCE events/cell detected in the $TOP3A^{-/-}$ and wild type cells, respectively. Meanwhile, SCEs increased by almost 5.0 and 4.2-fold in the *BLM* and *RMI2* knockout cells, respectively, compared with wild type cells ($p < 0.0001$ for both cells; average 30.4 and 26.0 SCE events/cell in $BLM^{-/-}$ and $RMI2^{-/-}$ cells, respectively). These data are consistent with previous reports[15, 16]. Interestingly, elevated SCEs was significant lower in HCT116 $TOP3A^{-/-}$ cells than in either *BLM* or *RMI2* knockout cells ($p < 0.0001$ and $p = 0.0021$, respectively; Fig. 3c).

The combination of moderate increase of SCEs and moderate decrease of cell proliferation in $TOP3A^{-/-}$ cells suggested a milder impact of TOP3A on genome instability. As a DNA repair disorder, Bloom syndrome patients are mildly sensitive to sunlight and display sun-sensitive lesions on exposed areas, such as the face, while no cutaneous photosensitivity was shown in reported *RMI1*, *RMI2*, or *TOP3A* deficient patients[15, 16]. The affected siblings reported in this study also displayed no sign of sun-sensitive problems. The HCT116 *TOP3A* null cells also did not show any UV sensitivity compared to the parental wide type cells (data known shown).

3.3 TOP3A-D479G retains the function on genome stability.

To test whether the mutant TOP3A (TOP3A-D479G) retained the enzymatic activity as wildtype TOP3A, we generated several isogeneic cell lines based on the HCT116-TOP3A knock out cells, in which the V5- or EGFP-tagged TOP3A proteins (wildtype and mutant) were stably expressed. As shown in Fig. 4b, protein expression levels of the BTR complex, including BLM, RMI1, and RMI2, were restored in HCT116-$TOP3A^{-/-}$ cells that stably expressed both wildtype (TOP3A-WT-V5) and mutant (TOP3A-D479G-V5) TOP3A. Cell proliferation assays were then performed; overexpression of both TOP3A-WT-V5 and TOP3A-D479G-V proteins rescued the growth/mitotic failure observed in $TOP3A^{-/-}$ HCT116 cells (Fig. 4c). Moreover, the elevated SCEs detected in $TOP3A^{-/-}$ cells were also ameliorated by adding back TOP3A-WT-V5 or TOP3A-D479G-V5 proteins (Fig. 4d). Taken together, these results

suggest that TOP3A-D479G retained the catalytic activity, which is mainly important for the double-Holliday-junctions dissolution in cells. To explain the cytological defects of elevated SCEs and reduced cell proliferation in the affected patient, we set out to detect cellular localization as well as protein stability of TOP3A-D479G with cells that stably expressed with GFP-TOP3A-D479G or GFP-TOP3A-WT. Unexpectedly, neither cellular localization change (Fig. 4a) nor reduced protein stability (**Supplemental Fig. 3b**) was shown in GFP-TOP3A-D479G expression cells.

3.4 TOP3A-D479G has defective mitochondrial respiratory function.

The effects of TOP3A mutations on mitochondrial function was first evaluated by measuring the cellular and mitochondrial ATP generation levels. Mitochondrial ATP levels were explored by subtracting the cytosolic ATP level from total cellular ATP levels. As shown in Fig. 5a, the contents of mitochondrial ATP in HCT116 *TOP3A*$^{-/-}$ cells were significantly lower than the mean value measured in the HCT116 WT cells (65.8% ± 17.6% of the WT, $p < 0.05$). Adding back wildtype TOP3A to HCT116 *TOP3A*$^{-/-}$ rescued its ATP production (102.6 ± 16.5% of the WT, $p > 0.05$). By contrast, the HCT116 *TOP3A*$^{-/-}$ cells expressing TOP3A-D479G remained deficient in ATP production. (73.4% ± 9.8% of WT, $p < 0.05$); no obvious change of cytosolic ATP level was observed.

The TOP3A-D479G effects on mitochondrial respiration was subsequently evaluated by a Seahorse Extracellular Flux analyser. In HCT116 *TOP3A*$^{-/-}$ cells, both basal and maximum oxygen OCR decreased compared to HCT116 WT cells (Fig. 5b), while transduction of the wildtype TOP3A but not TOP3A-D479G restored defects of both basal and maximum OCR.

We then performed transcriptome analyses to explore the reason of defective mitochondrial respiration. Compared with their parents, both the affected brother and the sister had significantly decreased expression of mitochondria-coding 15 genes in the peripheral blood (Table 1). Each of these 15 genes encodes a component of 4 enzyme complexes that form the mitochondrial respiratory chain (complex I, III, IV, and V), indicating impaired energy generation may be involved in pathogenesis of the siblings.

Table 1
Count per million of mitochondria-coding genes from peripheral bloods of this family by RNAseq method.

Gene Symbol	Ensembl gene type	Father	Mather	Brother	Sister	Mean logCPM	log2FC	p value	subunit of mitochondria respiratory chain
ENSG00000228253_MT-ATP8	Protein coding	185.6	150.1	32.6	53.8	6.72	-1.96	0.000	C
ENSG00000198695_MT-ND6	Protein coding	587.8	442.4	43.9	124.1	8.23	-2.62	0.000	C
ENSG00000212907_MT-ND4L	Protein coding	323.3	244.9	43.6	88.4	7.45	-2.11	0.000	C
ENSG00000198727_MT-CYB	Protein coding	1670.2	1177.8	165.8	301.1	9.69	-2.61	0.000	C
ENSG00000198840_MT-ND3	Protein coding	586.3	362.1	108.3	135.9	8.22	-1.96	0.000	C
ENSG00000198888_MT-ND1	Protein coding	2064.3	1285.7	173.1	412.8	9.94	-2.52	0.001	C
ENSG00000198786_MT-ND5	Protein coding	1763.2	1545.5	151.5	436.8	9.93	-2.49	0.001	C
ENSG00000198886_MT-ND4	Protein coding	3671.5	2413.4	352.0	657.7	10.79	-2.59	0.001	C
ENSG00000198938_MT-CO3	Protein coding	2871.9	1664.7	405.9	505.9	10.41	-2.31	0.002	C
ENSG00000198899_MT-ATP6	Protein coding	1896.1	1429.5	288.8	471.0	10.00	-2.13	0.003	C
ENSG00000211459_MT-RNR1	Mt rRNA	2413.1	1562.7	248.1	569.1	10.23	-2.28	0.003	
ENSG00000198763_MT-ND2	Protein coding	2575.5	1601.8	251.6	622.4	10.30	-2.26	0.004	C
ENSG00000198712_MT-CO2	Protein coding	3071.9	1894.4	484.3	769.5	10.60	-1.99	0.009	C
ENSG00000210082_MT-RNR2	Mt rRNA	6439.4	4026.2	877.3	1627.5	11.66	-2.06	0.015	
ENSG00000198804_MT-CO1	Protein coding	9079.7	5497.6	1051.8	2327.6	12.13	-2.11	0.019	C

3. Discussion

A syndrome with *TOP3A* deficiency is a recently reported human disease, with the Bloom-like phenotypes including severe pre- and postnatal growth deficiency and microcephaly[15, 17]. Here, we describe the entire disease courses of two siblings with *TOP3A* deficiency (Table 2, **supplemental Fig. 4**). They displayed Bloom-like features, including severe pre-and postnatal growth deficiency, small head, triangular face, feeding difficulties, as well as elevated SCEs on cytogenetic testing. Consistent with previously reported *TOP3A* deficiency patients, these siblings exhibited neither photosensitive molar rash nor cancer susceptibility until their decease, which are distinct from Bloom syndrome. Notably, these patients exhibited reduced subcutaneous fat and rapidly progressed cardiomyopathy, which are not common features in previously reported *TOP3A* deficiency patients.

Table 2
Clinical features of TOP3A-deficient siblings.

Feature	Bloom syndrome	RMI2 deletion	Brother	Sister
Prenatal growth retardation	+	-/+	+	+
Postnatal growth retardation	+	-/+	+	+
Decreased subcutaneous fat	+	-	+	+
Photosensitivity	+	-	-	-
Feeding difficulties	+	-	+	+
Gastro-esophageal reflux	+	-	-	-
Recurrent infections	+	-	-	-
Learning difficulties	+(variable)	-	-	-
Cancer onset in early adulthood	+	None at age 6/4	None at age 6	None at age 5
Diabetes	+	Not at age 6/4	None at age 6	None at age 5
Café-au-lait macules	+	++	-	-
Increased sister chromatid exchange	+	+	+	+
Fatty liver	-	-	+	+
Left hear failure	-	-	+	+
Elevated alpha-fetoprotein levels	-	+	+	+

The unique feature of these two siblings was that both of them developed hepatomegaly and the brother was confirmed to have fatty liver by liver biopsy and microscopic examination. We also found that both of these siblings had mildly elevated alpha-fetoprotein levels, which has been reported previously in patients with RMI2 deletion but not in either *TOP3A* deficiency or Bloom syndrome[15, 16]. Another different finding with prior report that recombinant human growth hormone did not significantly affect height of a patient with *TOP3A* deficiency[15], we observed good response to recombinant human growth hormone on the brother, which was suspended immediately on the finding of mildly elevated alpha-fetoprotein level. No apparent change in alpha-fetoprotein level was observed in his subsequent follow-ups until decease (Table 2).

The compound heterozygous mutations in the *TOP3A* gene, were identified in both siblings. One mutation is predicted to lead to a prematurely truncated protein, while another one is a missense mutation, TOP3A-D479G. To confirm the pathogenicity of the *TOP3A* mutations, functional studies on genome stability were performed using both patient blood and generated knockout cell lines. Cryogenic testing with the sister showed increased SCEs, suggesting impaired BTR complex function upon *TOP3A* mutation. However, adding back the TOP3A-D479G to HCT116 *TOP3A*$^{-/-}$ cells rescued expression of the BTR complex, as well as impaired cell proliferation and SCE events. Moreover, no obvious change of cellular localization or protein stability was found after induction of TOP3A-D479G, indicating that pathways other than BTR complex-mediated genome instability may have participated in the pathogenesis of our affected patients. We could not completely exclude the possibility that over-expression of TOP3A-D479G may decrease the impact on genome stability. Intriguingly, despite the severe phenotype of *TOP3A*-deficiency patients, less elevated SCEs and decreased cell proliferation was observed in HCT116-TOP3A$^{-/-}$ cells, compared with *BLM*$^{-/-}$ cells, further indicating other pathways may be involved in the pathogenicity of the *TOP3A*-deficiency disorder.

The mitochondrial isoform of TOP3A, which functions independently of the BTR complex, is required for the mammalian mitochondrial genome (mtDNA) maintenance, and *TOP3A* deficiency was previously associated with characters of primary mitochondrial dysfunction, such as dilated cardiomyopathy, mitochondrial DNA depletion in muscle, progressive external ophthalmoplegia[15, 17, 18, 23]. As expected, TOP3A-D479G failed to restore the defects of the mitochondrial ATP production and the oxygen consumption rate detected in *TOP3A*$^{-/-}$ cells. Furthermore, consistent with a previous report that depletion of TOP3A

lead to loss of mtDNA copy number[17], the two siblings had universally decreased expression of mtDNA-coding genes, which encode enzymes of the mitochondrial respiratory chain (Table 1). The fatty liver observed on these two siblings was also presumed to be secondary the defect of mitochondrial function.

Respiratory chain dysfunction has been the main feature of patients with mitochondrial diseases and a mitochondrial drug cocktail has been applied clinically and proved to be effective [24, 25]. Since *TOP3A* deficiency patients have overlapped clinical phenotypes with mitochondrial disease, indicating the treatment options for mitochondrial diseases may be worthy of trial for *TOP3A* deficiency.

4. Conclusions

In conclusion, we reported two new siblings of TOP3A deficiency with new visceral organ involvement. The mitochondrial dysfunction induced by TOP3A deficiency may play a more important role than its effect on nuclear function in disease pathophysiology. The precise understanding of this pathophysiology would pave the way to find a cure for this rare and devastating disorder and even for some common diseases, such as aging.

5. Materials And Methods

5.1. Human studies

The family was recruited with the approval of the Ethics Committee at the Xinhua Hospital Affiliated to Shanghai Jiao Tong University School of Medicine, Shanghai, China (ethics approval number XHEC-C-2017-066). Written consent to join this study was obtained from the parents.

5.2. Next generation sequencing and Sanger sequencing

Peripheral blood samples were collected from the siblings and their parents. Genomic DNA was extracted using Lab-Aid Nucleic Acid Isolation Kit (Zeesan). SureSelect Human All Exon V5 kit (Agilent) was used to enrich protein coding regions for a library preparation of whole exome sequencing. The resulting libraries were sequenced on the HiSeq 4000 platform (Illumina) for paired-end 150-bp reads. Fastq-format reads were aligned to the human reference genome (hg19) using BWA-0.7.10. BAM files were manipulated using Picard tools-1.124. Base calling was performed following GATK best practice version 3. Quality metrics were evaluated, specifically, the depth was 87.8 per sample, with 98.2% of the target region covered by > 10 × reads. Subsequently, the vcf files were annotated using SnpEff version 4.2. Variants with > 1% frequency in the population variant databases-1000Genomes Project, Exome Variant Server (EVS) and Exome Aggregation Consortium (ExAC) or > 5% frequency in the local database with 150 exome datasets filtered. The intergenic, intronic, and synonymous variants were also filtered, except those located at canonical splice sites. Candidate variants were evaluated in the context of clinical presentation and inheritance mode. Selected variants were validated by Sanger sequencing in the proband and parents.

5.3. RNAseq of peripheral blood of family members

RNA purification, reverse transcription, library construction and sequencing were performed at WuXi NextCODE in Shanghai according to the manufacturer's instructions (Illumina). Briefly, polyA mRNA was purified from total RNA of the family (Brother, sister, the father and the mother) using oligo-dT-attached magnetic beads and then was fragmented. Taking these short fragments as templates, first strand cDNA was synthesized using reverse transcriptase and random primers, followed by second strand cDNA synthesis. Then the synthesized cDNA was subjected to end-repair, phosphorylation and 'A' base addition according to Illumina's library construction protocol. Then Illumina sequencing adapters were added to both sides of the cDNA fragments. After PCR amplification for DNA enrichment, the target fragments of 200–300 bp were cleaned up. After library validation, Illumina cBOT cluster generation system with HiSeq PE Cluster Kits was used to generate clusters. Paired-end sequencing was performed using an Illumina HiSeq system following Illumina-provided protocols for 2 × 150 paired-end sequencing.

5.4. Allele-specific quantitative RT-PCR

Total RNA was extracted using the RNeasy Plus Mini Kit (QIAGEN). The High-capacity RNA-to-cDNA kit (Applied Biosystems) was used for 1st strand synthesis. Quantitative PCR was performed using the Thermal Cycler Dice Real-Time system (TaKaRa Bio) with a QuantiTect SYBR Green PCR Kit (QIAGEN). An allele-specific quantitative RT-PCR was carried out using primers that selectively amplify the wildtype (WT) or the mutant *TOP3A* cDNAs from patients' peripheral blood. For each sample, relative mRNA expression levels were normalized using the *HPRT1* gene (**Supplemental Figure S1**). The primer sequences would be provided on request. Error bars represent standard error of means from triplicate experiments.

5.5. Sister chromatid exchange assay (SCE)

Fresh blood cells were cultured for three days in RPMI 1640 media with 10% FBS and phytohaemagglutin (20 μg/ml). BrdU (Sigma-Aldrich) was added to a final concentration of 10 μg/ml for 30 hours. Cells were then treated with colcemid (0.1 mg/ml, 45 min, Sigma-Aldrich) prior to standard metaphase chromosome harvest. Slides were placed in a biosafety cabinet and were exposed to UV light at a distance of 30 cm for 45 min. Slides were rinsed in ddH_2O and stained in Leishman's stain (Sigma-Aldrich).

For HCT116 cell lines, 30% confluent cells were treated for 35 h with 10 μM BrdU, followed by colcemid (0.15 μg/ml, minimum 1 h, Sigma) to enrich mitotic cells. Metaphases and nuclei were isolated in hypotonic buffer (75 mM KCl), fixed with fixative (3:1 solution of methanol: glacial acetic acid) and dropped onto pre-chilled slides. Dried slides were stained with acridine orange (0.1 mg/ml in MilliQ water, 2 min, Molecular Probes), then extensively washed and mounted with Sorenson buffer (pH 6.8, Sigma).

5.6. Cell culture

Human colon cancer HCT116 (RCB2979) cells were purchased from the RIKEN BRC. All cell lines used in this study were cultured in DMEM (Dulbecco's Modified Eagle Medium, Wako) complemented with 10% FBS (Fetal Bovine Serum, GIBCO) and 1 × penicillin-streptomycin **(**Wako). Cells were cultured at 37 ºC in 5% CO_2 atmosphere.

5.7. Knock out cell lines

TOP3A, *RMI2*, and *BLM* knock out HCT116 cell lines were generated by CRISPR-Cas9 techniques. Briefly, guide RNA (gRNA) targeting the exonic region of indicated genes were designed at http://chopchop.cbu.uib.no (**Supplemental Figure S2**). The CRISPRs were generated in single plasmid containing both sgRNA and the Cas9 (pSpCas9(BB)-2A-Puro (px459, Addgene). After 24 h post-transfection, cells were subjected to puromycin selection (2 μg/ml) for further 48 h. Single cell cloning of survived cells was performed by limit dilution in 96-well plates. After 2–3 weeks individual clones were picked and expanded for genotyping. Genomic DNA of selected clones were extracted by MightyAmp Genotyping Kit (R074A, TAKARA) according to the manufacturer's instructions. A 350 ~ 450 base pair region around the expected cleavage site of targeted genes were amplified, which were subject to Sanger sequencing (Eurofins genomics). The lack of protein expression in selected cell clones were further confirmed by Western Blotting.

5.8. Lentivirus experiments

Experiments were performed as described previously[20]. Recombinant lentivirus particles expressing the C-terminal V5-tagged *TOP3A* and the single amino-acid substitution mutant (*TOP3A-D479G*) were produced and used to infect the TOP3A-KO cell lines. Sequence of the mutant plasmid was confirmed by Sanger sequencing (**Supplemental Figure S3A**). Forty-eight hours after lentiviral infection, blasticidin (10 μg/ml, Sigma-Aldrich) was added to the medium for selection of TOP3A stably expressing cells. Single cell cloning of survived cells was performed by limit dilution in 96-well plates. After 2 to 3 weeks, individual clones were picked and expanded, and V5-TOP3A protein expression was examined by Western Blotting.

5.9. Protein stability

HCT116 cells were transiently transfected with GFP-tagged TOP3A or its mutant plasmid. Cells were treated with cycloheximide (100 μg/ml) then harvested at the indicated time points. Whole cell lysate was analyzed by Western blotting using anti-GFP antibody.

5.10. Confocal fluorescence microscopy

HCT116 cells transiently expressing GFP-TOP3A or GFP-TOP3A-D479G were washed once with PBS (Wako) and fixed with Fix buffer [300 mM sucrose, 2% (v/v) formaldehyde, and 0.2% (v/v) Triton X-100 in PBS]. After a brief washing in PBS, cells were incubated with DAPI (10 ng/mL, 15 min). Cells were then washed, mounted, and examined on a LSM 700 laser scanning confocal microscope (Carl Zeiss). Images were taken with the 40 × oil immersion objective lens under identical imaging settings.

5.11 Mitochondrial ATP contents

ATP generation was measured using an ATP analysis kit (Beyotime) according to the manufacturer's instructions. Briefly, cells were treated with ATP synthase inhibitor oligomycin, which inhibited mitochondrial ATP generation allowing us to determine the cytosol ATP levels. The same number of cells were incubated in culture medium to determine total cellular ATP levels. After treatment with oligomycin (100 ng/ml, 30 min), all cells were homogenized and centrifuged (12000 ·*g*, 5 min, 4 ˚C), and 20 μl of supernatant were mixed with 100 μl of luciferase assay reagent. ATP levels were measured in a microplate reader (Wallac 1420 victor^2). Protein concentration was measured with a micro protein assay kit (Thermo Scientific). Mitochondrial contents were the total cellular ATP levels minus the cytosol ATP levels and were expressed as nmol/mg protein.

5.12 Mitochondrial respiration

The impact TOP3A on oxygen consumption rate of HCT116 was measured in an XF^{e}96 extracellular flux analyzer (Seahorse Biosciences). Cells were plated at 10,000 cells/80 μl well in 96-well assay plates for 24 h. On the day of analysis, cells were changed to assay medium, which consisted of XF Base DMEM Medium supplemented with 10 mM glucose (Sigma), 2 mM sodium Pyruvate (Sigma), and 2 mM glutamine (pH 7.4), followed by equilibration at 37 ˚C in a non-CO_2 incubator for 1 h. Basal oxygen consumption rate was measured, then treatments were added sequentially: 1 μM oligomycin, a complex V inhibitor; 0.5 μM FCCP, a proton gradient uncoupler that collapses proton electrochemical gradients and allows respiratory chain to operate maximally; and 0.5 μM rotenone/antimycin, a complex I inhibitor. Oxygen consumption rates were automatically recorded and calculated by the Seahorse software.

5.13 Reagents and antibodies

Antibodies used were: TOP3A (14525-1-AP, Proteintech Group), BLM (ab2179, Abcam), RMI1 (A300-631A, Bethyl), RMI2 (ab122685, Abcam), V5-tag (ab95038, Abcam), GFP-tag (ab6556, Abcam), β-actin (sc-47778, Santa Cruz Biotechnology), Alpha-tubulin (Invitrogen), MG132, and cycloheximide (Sigma-Aldrich).

Abbreviations

BTR BLM-TOP3A-RMI1/2

mtDNA mitochondrial DNA

OCR oxygen consumption rate

SCEs sister chromatid exchanges

Declarations

6.1. Ethics approval and consent to participate

The study has been approved by the Institutional Review Ethics Board of the Shanghai Xinhua Hospital, Shanghai Jiao Tong University School of Medicine. The parents provided written informed consent form to join this study.

6.2. Consent for publication

Written informed consent was obtained from all participants.

6.3. Availability of data and supporting materials section.

The datasets used and/or analysed during the current study are available from the corresponding author on reasonable request.

6.4. Competing interests

The authors declare that they have no conflict of interest.

6.5. Funding

This project is supported by Shanghai Municipal Education Commission-Gaofeng Clinical Medicine Grant Support (20152520), Shanghai Science and Technology Committee (19140904100), NSFC (81570516), National Key Research and Development Program (2016YFC0905100, 2016YFC0901505).

6.6. Contributions

Study design: WJ, NJ, CG, JW and LW, Data collection and data analysis; NJ, CG, HZ and TO drafted manuscript; all authors approved final version of manuscript; HZ and TO designed the study and takes responsibility for the integrity of the data analysis.

6.7. Acknowledgements

The authors thank the patient and their guardians to be included in this study.

References

1. Landau JW, Sasaki MS, Newcomer VD, Norman A. Bloom's syndrome. The syndrome of telangiectatic erythema and growth retardation. Archives of dermatology. 1966;94(6):687–94.
2. Landau J, Katzenellenbogen I, Laron Z. Eye findings in congenital telangiectatic erythema and growth retardation (Bloom's syndrome). Am J Ophthalmol. 1966;62(4):753–4.
3. Bouman A, van Koningsbruggen S, Karakullukcu MB, Schreuder WH, Lakeman P. Bloom syndrome does not always present with sun-sensitive facial erythema. European journal of medical genetics. 2017.
4. Renes JS, Willemsen RH, Wagner A, Finken MJ, Hokken-Koelega AC. Bloom syndrome in short children born small for gestational age: a challenging diagnosis. J Clin Endocrinol Metab. 2013;98(10):3932–8.
5. Chisholm CA, Bray MJ, Karns LB. Successful pregnancy in a woman with Bloom syndrome. Am J Med Genet. 2001;102(2):136–8.
6. Singh TR, Ali AM, Busygina V, Raynard S, Fan Q, Du CH, Andreassen PR, Sung P, Meetei AR. BLAP18/RMI2, a novel OB-fold-containing protein, is an essential component of the Bloom helicase-double Holliday junction dissolvasome. Genes Dev. 2008;22(20):2856–68.
7. Xu D, Guo R, Sobeck A, Bachrati CZ, Yang J, Enomoto T, et al. RMI, a new OB-fold complex essential for Bloom syndrome protein to maintain genome stability. Genes Dev. 2008;22(20):2843–55.
8. Wu L, Bachrati CZ, Ou J, Xu C, Yin J, Chang M, et al. BLAP75/RMI1 promotes the BLM-dependent dissolution of homologous recombination intermediates. Proc Natl Acad Sci U S A. 2006;103(11):4068–73.
9. Raynard S, Bussen W, Sung P. A double Holliday junction dissolvasome comprising BLM, topoisomerase IIIalpha, and BLAP75. J Biol Chem. 2006;281(20):13861–4.
10. Yin J, Sobeck A, Xu C, Meetei AR, Hoatlin M, Li L, Wang W. BLAP75, an essential component of Bloom's syndrome protein complexes that maintain genome integrity. EMBO J. 2005;24(7):1465–76.
11. Wu L, Davies SL, North PS, Goulaouic H, Riou JF, Turley H, Gatter KC, Hickson ID. The Bloom's syndrome gene product interacts with topoisomerase III. J Biol Chem. 2000;275(13):9636–44.

12. Johnson FB, Lombard DB, Neff NF, Mastrangelo MA, Dewolf W, Ellis NA, et al. Association of the Bloom syndrome protein with topoisomerase IIIalpha in somatic and meiotic cells. Cancer Res. 2000;60(5):1162–7.
13. Hickson ID. RecQ helicases: caretakers of the genome. Nat Rev Cancer. 2003;3(3):169–78.
14. Ray JH, German J. Bloom's syndrome and EM9 cells in BrdU-containing medium exhibit similarly elevated frequencies of sister chromatid exchange but dissimilar amounts of cellular proliferation and chromosome disruption. Chromosoma. 1984;90(5):383–8.
15. Martin CA, Sarlos K, Logan CV, Thakur RS, Parry DA, Bizard AH, et al. Mutations in TOP3A Cause a Bloom Syndrome-like Disorder. Am J Hum Genet. 2018;103(2):221–31.
16. Hudson DF, Amor DJ, Boys A, Butler K, Williams L, Zhang T, Kalitsis P. Loss of RMI2 Increases Genome Instability and Causes a Bloom-Like Syndrome. PLoS Genet. 2016;12(12):e1006483.
17. Nicholls TJ, Nadalutti CA, Motori E, Sommerville EW, Gorman GS, Basu S, et al. Topoisomerase 3alpha Is Required for Decatenation and Segregation of Human mtDNA. Molecular cell. 2018;69(1):9–23 e26.
18. Wang Y, Lyu YL, Wang JC. Dual localization of human DNA topoisomerase IIIalpha to mitochondria and nucleus. Proc Natl Acad Sci U S A. 2002;99(19):12114–9.
19. Mo D, Zhao Y, Balajee AS. Human RecQL4 helicase plays multifaceted roles in the genomic stability of normal and cancer cells. Cancer letters. 2018;413:1–10.
20. Jia N, Nakazawa Y, Guo C, Shimada M, Sethi M, Takahashi Y, Ueda H, Nagayama Y, Ogi T. A rapid, comprehensive system for assaying DNA repair activity and cytotoxic effects of DNA-damaging reagents. Nat Protoc. 2015;10(1):12–24.
21. Li W, Wang JC. Mammalian DNA topoisomerase IIIalpha is essential in early embryogenesis. Proc Natl Acad Sci U S A. 1998;95(3):1010–3.
22. Grierson PM, Lillard K, Behbehani GK, Combs KA, Bhattacharyya S, Acharya S, Groden J. BLM helicase facilitates RNA polymerase I-mediated ribosomal RNA transcription. Hum Mol Genet. 2012;21(5):1172–83.
23. Viscomi C, Zeviani M. MtDNA-maintenance defects: syndromes and genes. J Inherit Metab Dis. 2017;40(4):587–99.
24. Hanna MG, Nelson IP. Genetics and molecular pathogenesis of mitochondrial respiratory chain diseases. Cell Mol Life Sci. 1999;55(5):691–706.
25. Omata T, Fujii K, Takanashi J, Murayama K, Takayanagi M, Muta K, et al. Drugs indicated for mitochondrial dysfunction as treatments for acute encephalopathy with onset of febrile convulsive status epileptics. J Neurol Sci. 2016;360:57–60.

Figures

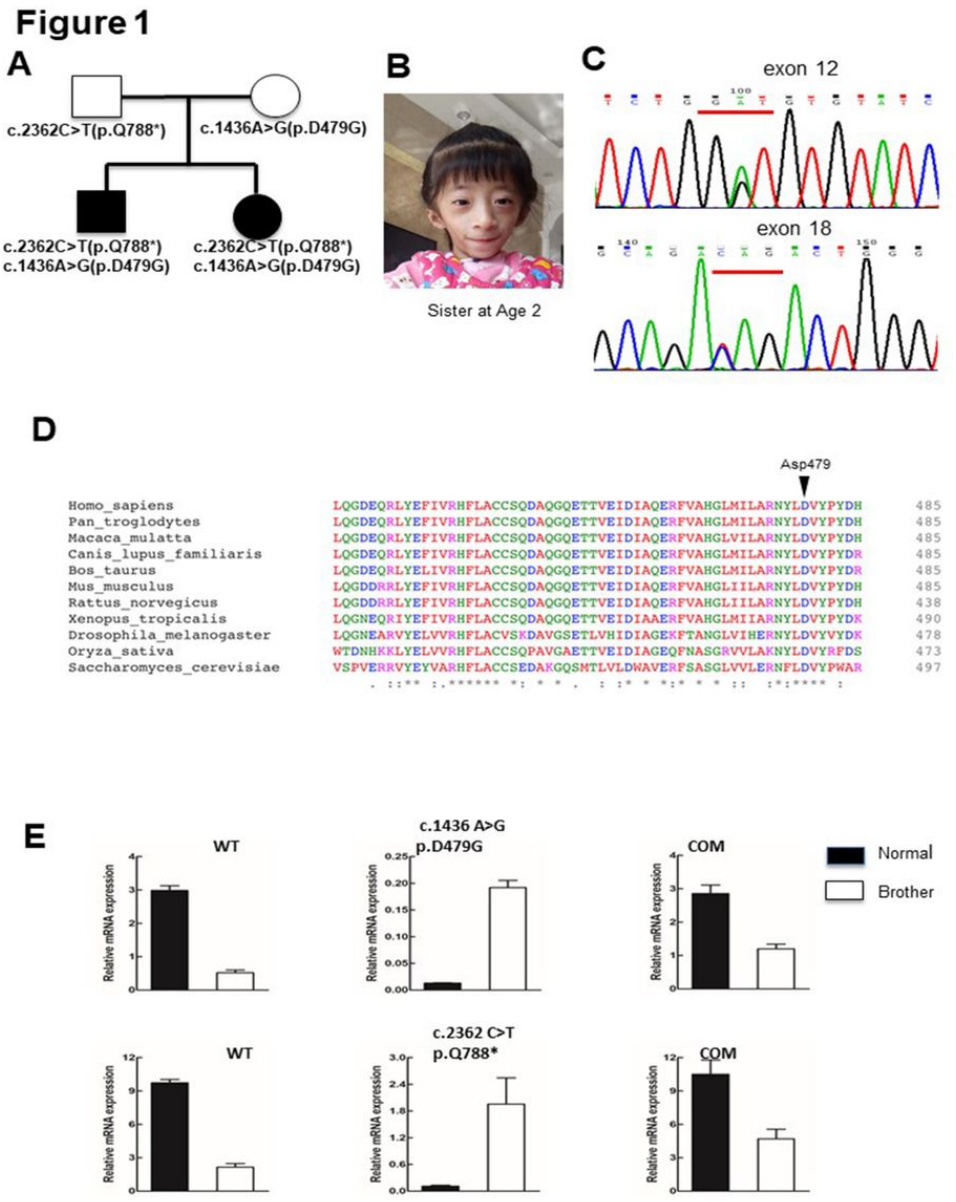

Figure 1

Identification of mutations in the TOP3A gene in a family. (A)The family tree of our patients. (B) Clinical pictures of the sister with TOP3A mutations at the age of 2 year. (C) Genome DNA Sanger sequencing confirmed that the siblings carried the compound heterozygous mutations in the TOP3A gene. One mutation is the c.1436A>G in exon 12, which caused a missense mutation p. D479G. The other one is the c.2362C>T in exon 18, which resulted in a premature stop gain at p.Q778*. The altered nucleotides are marked by red bars. (D) Conservation analysis of the TOP3A sequence by using ClustalOmega showed that Asp479 in TOP3A is highly conserved in eukaryotes. (E) Selective quantitative amplification of the wild type (WT) and each mutational allele in peripheral blood cells collected from the brother. The HPRT1 gene served as a quantification control.

Figure 2

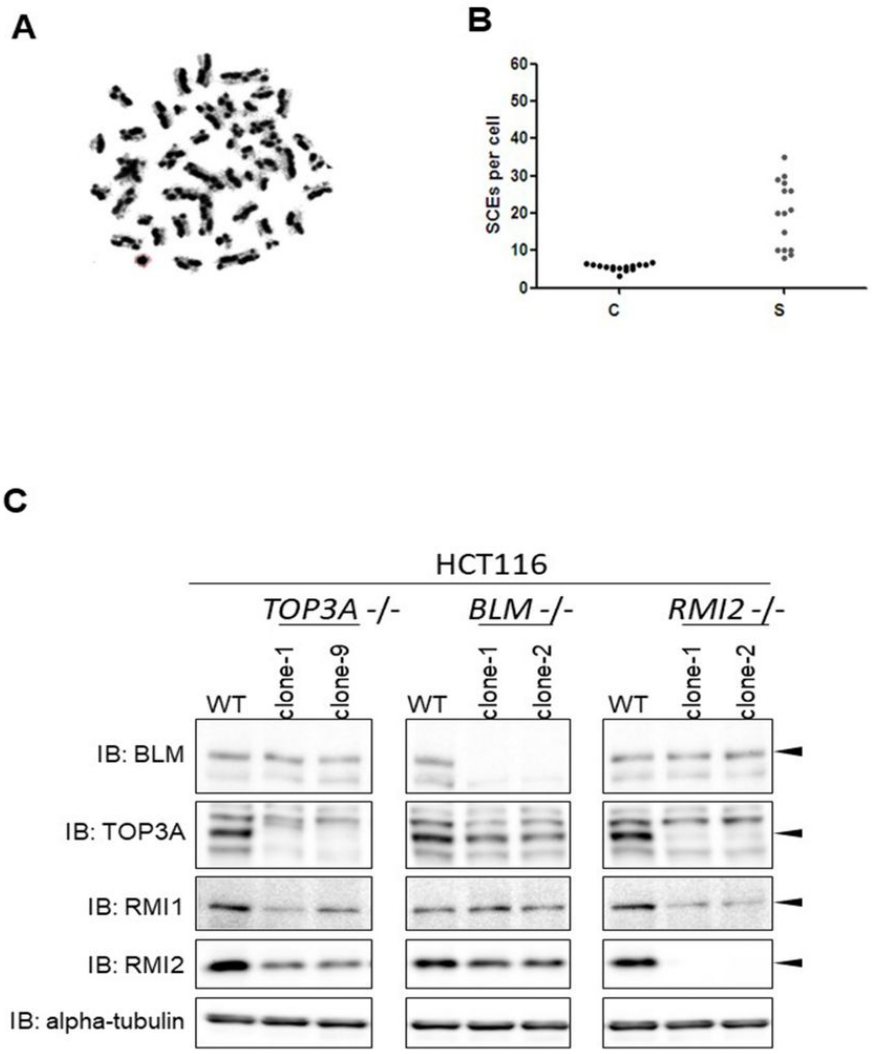

Figure 2

Patients carrying the TOP3A mutations showed increased SCE events. (A, B) BrdU stand-specific labelling of sister chromatids showed that patient blood cells had more SCE events than control cells. C, control cells; S, patient cells. (C) Immunoblotting of TOP3A, BLM, and RMI1/2 proteins in generated HCT116 knock out cell lines with alpha-tubulin as a loading control. The black solid arrows indicate the position of each protein.

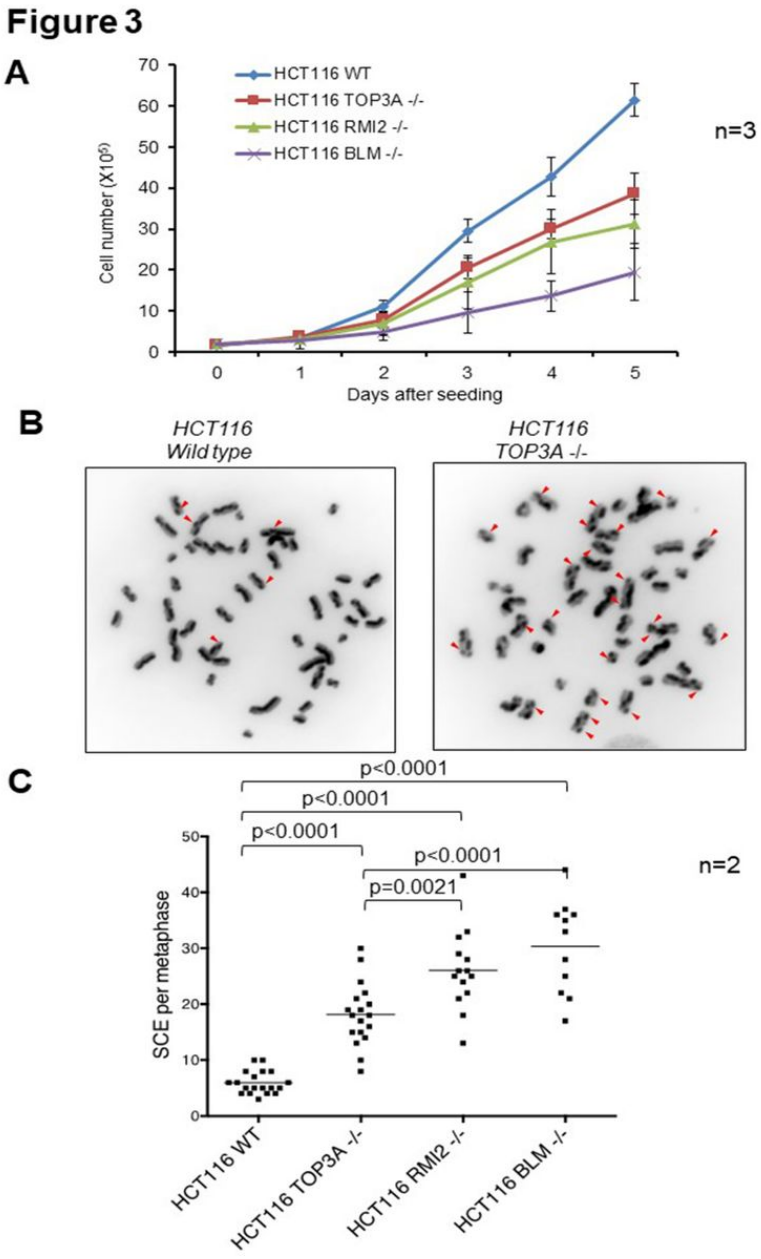

Figure 3

Knock out of TOP3A gene in cells showed BLM-like cellular phenotypes. (A) Cell proliferation analyses were carried out over 5 days in each generated knock out (KO) cell lines, error bars represent standard error from triplicate experiments. (B, C) Sister chromatid exchange analysis on parental (wild type) and HCT116-TOP3A-KO cell lines, the red arrows indicate exchange sites. Fifteen to twenty metaphase cells were analyzed for each KO cell line, quantification of SCE events was shown in (C). Error bars represent standard error of the mean from two independent experiments. One-way ANOVA was performed against parental control cells.

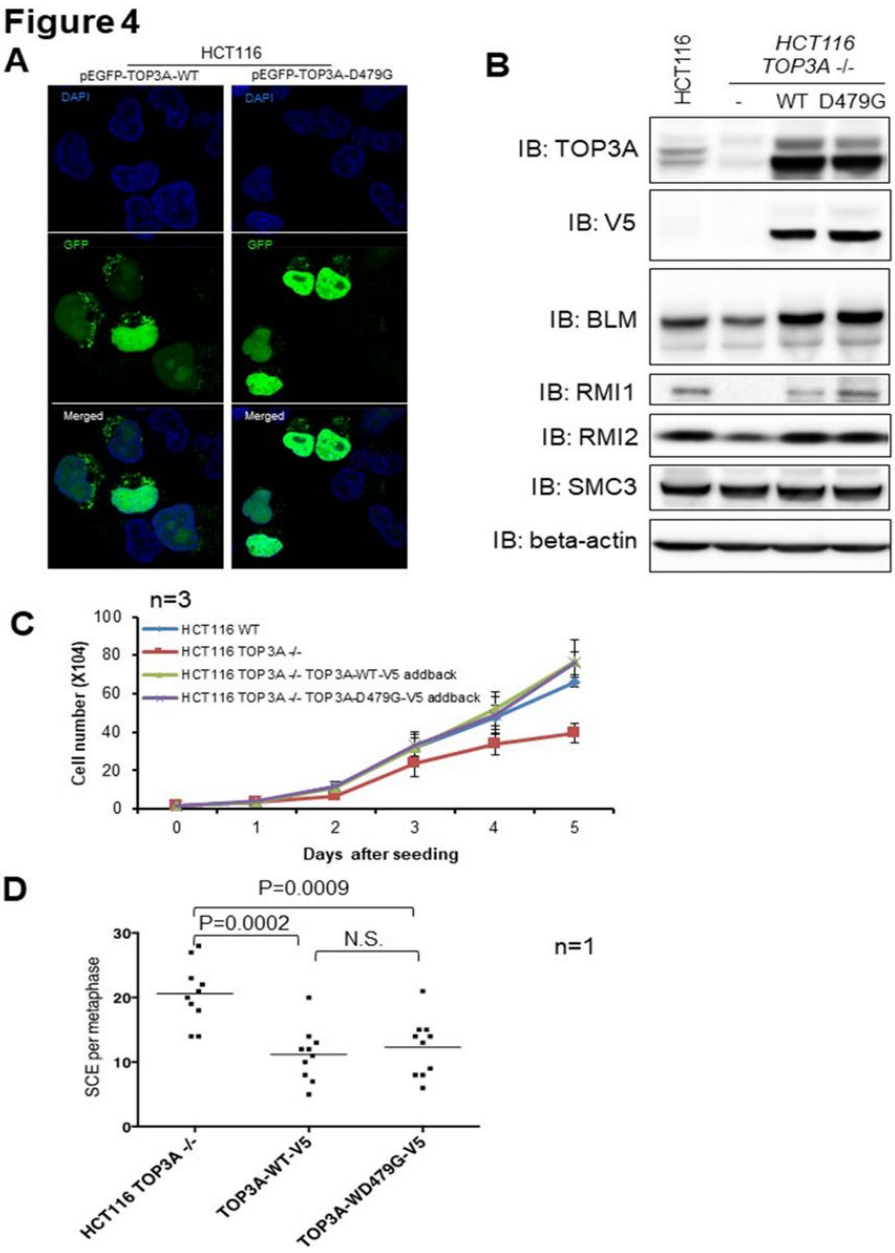

Figure 4

Ectopic expression of TOP3A proteins in TOP3A-/- cells. (A)Cellular localization analysis using HCT116-TOP3A-KO cell lines that stably express GFP-tagged TOP3A-WT and TOP3A-D479G proteins. Cells were fixed and DAPI-stained (blue); Merged, merged picture. (B, C, D) Functional analysis with HCT116-TOP3A-KO cell lines that stably expressed V5-tagged TOP3A-WT and TOP3A-D479G proteins. Immunoblots showed overexpression of WT and mutant TOP3A proteins restored expression of BTR complex proteins (B). Re-introduction of WT and mutant TOP3A proteins rescued the cell proliferation defects (C) and the abnormal SCE (D) observed in HCT116-TOP3A-KO cells. Error bars represent standard error of the mean.

Figure 5

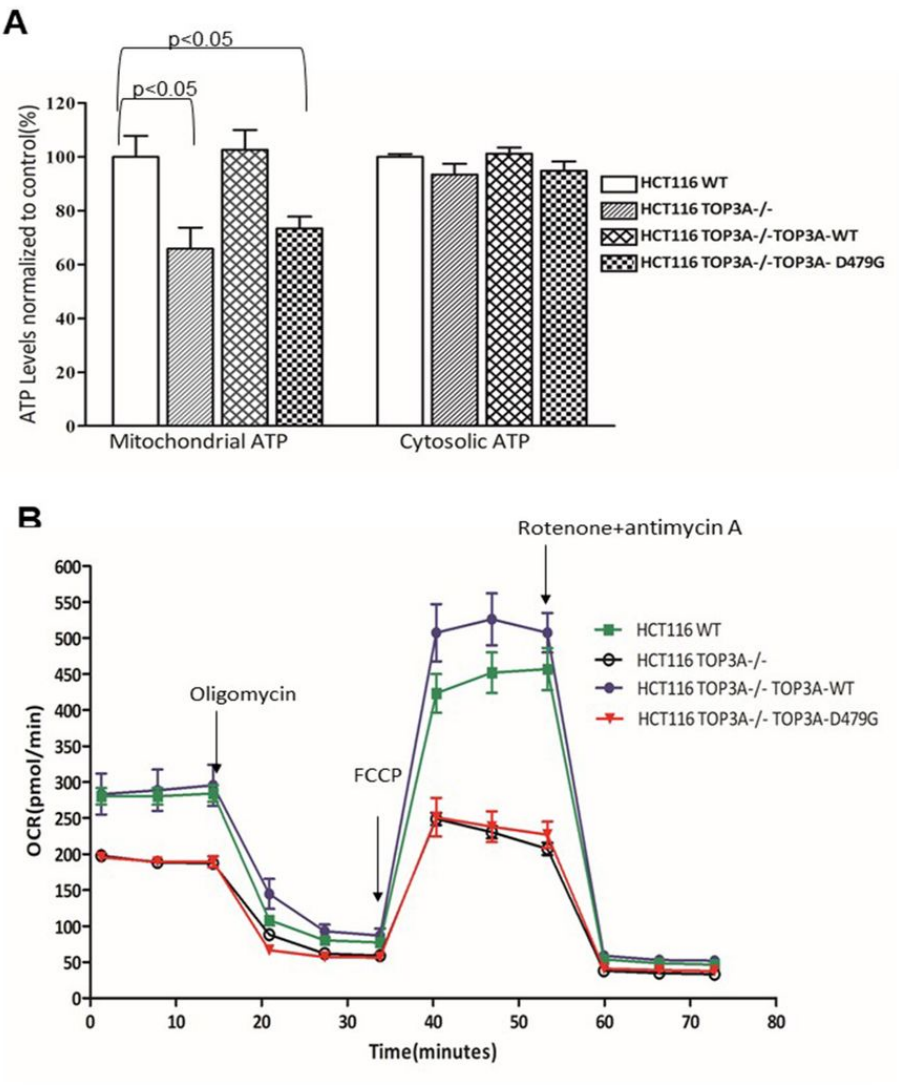

Figure 5

D479 in TOP3A may be involved in functional maintenance of mitochondria. (A) Sub-cellular ATP levels were analyzed in indicated cell lines. Cells were subcellular fractionated and both mitochondrial and cytosolic ATP levels were measured. Expression of TOP3A-WT, but not TOP3A-D479G, specifically restored mitochondrial ATP levels in HCT116-TOP3A-KO cells. (B) The seahorse cell mito stress tests were performed to measure oxygen consumption rate (OCR) of indicated cell lines. Arrows indicate when specific stressors were added: oligomycin, carbonyl cyanite-4 (trifluoromethoxy) phenylhydrazone (FCCP), and rotenone. Error bars represent S.D. obtained from triplicate experiments.

Supplementary Files

This is a list of supplementary files associated with this preprint. Click to download.

- growthchartsupplementrayfigure.jpg
- renamed67f29.JPG
- renamed55e31.JPG

- renamedd31e5.JPG